Journal of Sound and Vibration (1997) **204**(5), 769–794

NON-UNISON DYNAMICS OF MULTIPLE CENTRIFUGAL PENDULUM VIBRATION ABSORBERS

C.-P. Chao, C.-T. Lee and S. W. Shaw

Department of Mechanical Engineering, Michigan State University, East Lansing, MI 48824, *U.S.A.*

(*Received* 22 *July* 1996, *and in final form* 13 *January* 1997)

Centrifugal pendulum vibration absorber (CPVA) systems are used to decrease steady state torsional vibration levels and extend operating ranges for rotating and reciprocating machinery. They are typically sized and designed for a given harmonic using the assumption that a set of identical absorbers move in exact unison. Herein an investigation is carried out to determine the consequences, in terms of system performance, of a recently uncovered dynamic instability of this unison motion. The system considered consists of a rigid rotor and N CPVA's riding on epicycloidal paths tuned to order n, the same as the dominant order of the applied torque. Using two co-ordinate transformations and the method of averaging, the system dynamics can be modelled by a set of $2N$ first order, internally resonant, autonomous differential equations. A bifurcation analysis of these equations shows that the post-bifurcation dynamics, in which a single absorber moves out of step with its partners, is dynamically stable and leads to the worst-case (that is, the smallest) operating torque range. Furthermore, it is found that the rotor acceleration undergoes a mild saturation, leading to slightly improved performance beyond the instability. Analytical estimates of the torque range and the rotor acceleration are derived based on a truncated version of the equations, and more accurate estimates are obtained from a numerical solution of the non-truncated equations. The results are compared with numerical simulations.

1. INTRODUCTION

In the dynamics of rotating and reciprocating machinery, forces are often generated that cause undesirable oscillatory torques at frequencies that are multiples of the nominal rotation rate. These torques result in torsional oscillations which introduce roughness and fatigue difficulties. The CPVA is a passive device used for reducing such torsional oscillations in a rotating system. It consists essentially of a mass whose center of gravity (C.G.) is restricted to move along a prescribed path relative to the base rotating system. This mass is driven by the dynamics of the rotor, and its motion provides a restoring torque which, when the path is properly designed, reduces the level of torsional oscillations of the rotor.

CPVA's were invented for use in internal combustion engines as early as 1929 [1] and have been successfully employed to suppress torsional vibrations in light aircraft engines and helicopter rotors [2]. Previous analytical works [3–5] have concentrated on analyzing the non-linear dynamics of CPVA's which use the easily manufactured circular paths for the absorber kinematics. Improved performance of CPVA's can be achieved by intentional mistuning of circular paths at small amplitudes and/or by accounting for the system's

0022–460X/97/300769 + 26 $25.00/0/sv970960

nonlinear dynamic behavior over the entire amplitude range. For example, as shown in references [6–10], the use of non-circular paths can be quite effective in reducing the level of torsional oscillations over a large torque range. It is interesting to note that the aforementioned designs are based on the assumption that the absorber system for addressing a given harmonic consists of only a single dynamic mass.

However, in practice, due to spatial and balancing considerations, the implementation of CPVA's requires that the total absorber inertia be divided into several absorber masses that are stationed about and/or along the axis of rotation. If all absorbers move in exact unison, the usual design conclusions are valid. However, Chao *et al*. [11] have shown that for the epicycloidal absorber path, the unison motion of N identical absorbers may become unstable at a moderate level of the disturbing torque level, in which case the performance of the absorbers in the post-bifurcation stage becomes of interest. In addition, it was observed in simulations that the post-critical response involved $N-1$ absorbers moving in relative unison with the remaining absorber undergoing a larger amplitude motion.

The present study aims to uncover the source of this response and to determine the effects it has on system performance. To this end, the dynamic response of a rigid rotor fitted with N identical absorbers using epicycloidal paths and subjected to a harmonic torque is considered. The primary goal of this effort is to determine the nature and stabilities of the post-bifurcation, non-unison solutions in order to estimate the effects that the bifurcation has on the rotor acceleration and the operating torque range. It should be noted that the present results are only the first step in such a study, as some important issues must be considered in subsequent work in order for the results to be of any practical use. These matters are taken up in the conclusions.

The system under consideration has several identical subsystems that lead to inherent symmetries in the equations of motion. Therefore, concepts from group theory are adopted in order to analyze the post-bifurcation solutions. (The relevant symmetry group for the system is, in terms of standard notation, $\mathbf{S}_N$.) A linear transformation among absorber displacements is first performed to separate the dynamics into two invariant subspaces which are induced by the embedding symmetry of the system. These subspaces represent the unison response and its complement. A transformation to polar co-ordinates is then performed in order to conduct averaging. With the averaged equations in hand, different levels of expansion in the absorber amplitudes are investigated. The full, non-truncated results are very accurate, but require numerical solution of integrals and transcendental equations. By considering the equations truncated at the leading non-linear order, an analytical approximation of the worst-case operating torque range can be found. This estimate shows that the leading order terms of the angular acceleration of the rotor saturate as the torque amplitude is increased, and, remarkably, that they are independent of the particular post-bifurcation solution branch encountered. It is also found that the bifurcation dramatically reduces the feasible operating torque range. This occurs since one absorber will move with a significantly larger amplitude than the others, and this absorber will reach the physical limits of its motion at a much lower torque amplitude when compared with the unison response. (The symmetry group for this response is $\mathbf{S}_1 \times \mathbf{S}_{N-1}$.) The above predictions are confirmed by the non-truncated average equations and by direct simulations.

This paper is organized as follows. In section 2, the mathematical model is presented, the embedding symmetry is identified and the scaling required for asymptotic analysis is formulated. In section 3, a linear transformation is adopted among absorber displacements to separate the dynamics into the two invariant subspaces. By averaging and truncation, two versions of the averaged equations are then obtained. In section 4, the $\mathbf{S}_1 \times \mathbf{S}_{N-1}$ solution branches are proved to be stable and to lead to the worst-case operating torque

range. In section 5, the rotor acceleration and the feasible operating torque ranges are estimated. In section 6, detailed simulations are conducted and compared with the various approximations for specific numerical examples. In section 7, some conclusions and directions for future work are offered.

2. MATHEMATICAL MODEL

2.1. EQUATIONS OF MOTION

A simplified model involving only the absorbers and a rigid rotating inertia with an applied torque is considered. The system is shown schematically by the cross sectional view of the rotor in Figure 1. This dynamical system consists of a rotor of moment of inertia, I_d, with respect to the center of rotation, denoted by O, and N absorbers moving freely on prescribed paths relative to the rotor. Each individual absorber, denoted by a subscript i for the ith absorber, is considered to be a point mass with mass m_i. (For the common bifilar arrangement of absorbers, one can account for the moments of inertia of the absorbers about their respective C.G.'s by simply including them in I_d, as they rotate at the same rate as the rotor.) The path for each absorber is specified by the function $R_i = R_i(S_i)$, where R_i is the distance from the C.G. of the absorber to point O and S_i is an arc-length variable along the path defined relative to the rotating frame of reference, with its origin at the point where R_i reaches its maximum value, denoted by $R_{i0} = R_i(0)$. Thus, the nominal moment of inertia with respect to O for each absorber is defined by $I_i = m_i R_{i0}^2$. The path is designed to be symmetric with respect to $S_i = 0$; i.e., $R_i(S_i) = R_i(-S_i)$. An absorber system of total mass m_0 is assumed to be composed of N absorbers with equal individual masses $(1/N)m_0$. The resistance of the absorber along its path is modelled by an equivalent viscous damping coefficient $c_a = c_{ai}$ for each i. For this study the absorber path is specified by $R^2(S_i) = R_i^2(S_i) = R_0^2 - n^2 S_i^2$ with $R_{i0} = R_0$ for each i. Note that this path is an *epicycloidal* path which tunes the oscillating frequency of each absorber to be equal to that of the disturbing torque, even when the absorbers undergo large motions. This is the *tautochronic* absorber of reference [7].

Let θ denote the angular displacement of the rotor. The applied torque (including load torques) is assumed to be a nominal constant, T_0, plus a disturbing torque $T_\theta(\theta)$ which is periodic in θ. The disturbing torque is here assumed to be harmonic of order n, i.e., $T_\theta(\theta) = \hat{T}_\theta \sin(n\theta)$. (These torques arise from a variety of sources, including attached linkages, etc., and are generally periodic with several harmonics. Here only the harmonic for which the absorber system is designed is considered.) The nominal steady state

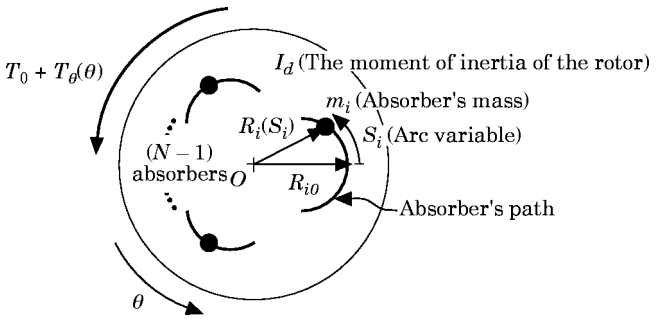

Figure 1. Cross-sectional schematic diagram of the rotor and absorbers.

rotational speed of the rotor, Ω, is the speed at which the constant torque T_0 balances the mean component of the torque which arises from rotational friction; thus,

$$\Omega = T_0/c_0, \tag{1}$$

where c_0 is the damping between the rotor and ground.

With the assumptions made, the overall system kinetic energy can be formulated. Assuming that gravitational effects are small compared to rotational effects and the corresponding potential energy is negligible, the governing equations of motion are determined by applying Lagrange's method to the kinetic energy. Introducing a new non-dimensionalized dependent variable y as

$$y \equiv \dot{\theta}/\Omega \tag{2}$$

and assuming that θ is a smooth and invertible function of t, these equations can be transformed into a set of periodically forced, non-autonomous equations with the independent variable θ replacing t. (This step transforms the non-linear term, $\hat{T}_\theta \sin(n\theta)$, into a periodic forcing term.) To simplify the mathematical model even further, non-dimensionalization is performed on the governing equations, yielding the following dynamical system that describes the dynamics of the N absorbers and the rotor:

$$y s_i'' + [s_i' + g(s_i)]y' + n^2 s_i y = -\hat{\mu}_a s_i', \qquad 1 \leqslant i \leqslant N, \tag{3a}$$

$$\frac{v}{N}\sum_{i=1}^{N}\left[-2n^2 s_i s_i' y^2 + (1 - n^2 s_i^2)yy' + g(s_i)s_i' yy' + g(s_i)s_i'' y^2 + \frac{\mathrm{d}g(s_i)}{\mathrm{d}s_i}\, s_i'^2 y^2\right] + yy'$$

$$= \frac{v}{N}\sum_{i=1}^{N}\hat{\mu}_a g(s_i)s_i' y - \hat{\mu}_0 y + \Gamma_0 + \hat{\Gamma}_\theta \sin(n\theta), \tag{3b}$$

where

$$(\,\cdot\,)' \text{ denotes } \mathrm{d}(\,\cdot\,)/\mathrm{d}\theta, \qquad s_i = S_i/R_{i0}, \qquad I_0 = m_0 R_0^2, \qquad v = I_0/I_d,$$

$$\hat{\mu}_a = c_a/m_i\Omega, \qquad \hat{\mu}_0 = c_0/I_d\Omega, \qquad \Gamma_0 = T_0/I_d\Omega^2, \qquad \hat{\Gamma}_\theta = \hat{T}_\theta/I_d\Omega^2,$$

$$g(s_i) = \sqrt{1 - (n^2 + n^4)s_i^2}, \qquad \frac{\mathrm{d}g(s_i)}{\mathrm{d}s_i} = -(n^2 + n^4)s_i/\sqrt{1 - (n^2 + n^4)s_i^2}. \tag{4}$$

Note that in terms of these dimensionless quantities, the steady rotation condition (1) becomes

$$\Gamma_0 = \hat{\mu}_0 \tag{5}$$

since the nominal steady value of y is unity.

The values of the function $g_i(s_i)$ must be kept real during absorber motions, and this leads to a restriction on the amplitudes of the absorber motions, given by

$$s_i(\theta) \leqslant s_{max} = 1/n\sqrt{n^2 + 1}, \qquad \forall\theta \qquad \text{and} \qquad \forall\ i. \tag{6}$$

This restriction keeps the absorber from passing the cusp points of the epicycloidal path. Note that the restriction in inequality (6) imposes a finite operating range on disturbing torque level, which is an important measure of the absorber system performance.

2.2. SYMMETRY IDENTIFICATION

Identifying the symmetry of the system allows one to search for and characterize the post-bifurcation solutions in an efficient way. Intuitively, due to the identical nature of each absorber, it is expected that the system described by equations (3a) and (3b) will enjoy some special properties. These properties can be mathematically characterized by transformations among the state variables that yield new sets of system equations which are both structurally and mathematically invariant from the original system equations. Such transformations are *symmetries* of the system. To mathematically characterize the symmetries of the system, conventional notation from group theory is employed. (See reference [12] for details.) Let

$$\dot{x} = h(x, \lambda) \tag{7}$$

be a system of first order differential equations, where x is a generalized state vector, λ is bifurcation parameter, and h: $\mathbf{R}^k \times \mathbf{R} \rightarrow \mathbf{R}^k$, is smooth. Let $\boldsymbol{\gamma}$ be an invertible $k \times k$ matrix representing a transformation among the state variables. It is said that $\boldsymbol{\gamma}$ is a symmetry of system (7) if

$$h(\boldsymbol{\gamma}x, \lambda) = \boldsymbol{\gamma}h(x, \lambda) \qquad \forall x \in \mathbf{R}^k. \tag{8}$$

It can be shown that system (7) is invariant subject to $\boldsymbol{\gamma}$ if equation (8) is satisfied. If there exists a group G such that the equation (8) is satisfied for each $\boldsymbol{\gamma} \in G$, then G is called a symmetry group of the system, or, equivalently, that the function h is called *G-equivariant*. To identify the symmetry group of the present model, first consider equation (3b), which describes the dynamics of the rotor. It is seen that the speed of the rotor, $y(\theta)$, is invariant subject to any permutation among the absorbers. Furthermore, from equation (3a), it can be confirmed that each absorber is coupled with all other absorbers only through y. Therefore, any permutation of absorbers should result in a system that is indistinguishable from the original. One can easily transform equations (3a) into $2N$ first-order differential equations and use the condition (8) to show that the symmetry group of the system is $\mathbf{S}_N$ (known as the "symmetric group" which is a group containing all permutations on N symbols [13]).

Based on group theory [12], there exist invariant subspaces in the absorber system due to the embedding symmetry $\mathbf{S}_N$. A partition of particular utility in the present work is

$$\mathbf{V} = \{\mathbf{s} \in \mathbf{R}^N \mid \mathbf{s} = [v, v, \ldots, v]^{\mathrm{T}}\} \qquad \text{and} \qquad \mathbf{W} = \mathbf{R}^N - \mathbf{V}, \tag{9}$$

where $\mathbf{V}$ is the subspace spanned by the unison mode and $\mathbf{W}$ is its complement. For any given initial conditions $s(0) \in \mathbf{V}$ or $s(0) \in \mathbf{W}$, the system dynamics will stay in $\mathbf{V}$ or $\mathbf{W}$, respectively, for all time.

It should be pointed out that bifurcations in systems with this level of symmetry can be extremely rich. In fact, due to the fact that many eigenvalues associated with $\mathbf{W}$ become simultaneously unstable, the corresponding bifurcation problem is highly degenerate and there may exist numerous branches of solutions emanating from a single bifurcation point. It is not always possible to determine all these branches, let alone their stability types. In the present case, measures of absorber performance are used in conjunction with symmetric bifurcation theory in order to get a handle on the most important branches, and in particular, the dynamically stable ones that limits the steady state system behavior.

2.3. SCALING CONSIDERATIONS

An approximation for the equations of motion and their solution is now provided that yields a form amenable to asymptotic analysis.

In most applications the ratio of the total nominal moment of inertia of all absorbers about point O to that of the entire rotating system is generally much smaller than one. This motivates the definition of the small parameter $\varepsilon \equiv \nu$ for asymptotic analysis. It is further assumed that the non-dimensional damping and excitation parameters, $\hat{\mu}_a$, $\hat{\mu}_0$, $\hat{\Gamma}_0$ and $\hat{\Gamma}_\theta$, are also small such that they can be scaled as follows:

$$\hat{\mu}_a = \varepsilon\tilde{\mu}_a, \qquad \hat{\mu}_0 = \varepsilon\tilde{\mu}_0, \qquad \Gamma_0 = \varepsilon\tilde{\Gamma}_0, \qquad \text{and} \qquad \hat{\Gamma}_\theta = \varepsilon\tilde{\Gamma}_\theta. \tag{10}$$

The unperturbed system dynamics for this case are determined by considering equation (3b) with $\varepsilon = 0$, that is, $\nu = 0$, which yields $y = 1$ (the constant value of y is fixed at unity by the non-dimensionalization employed). Using this in equation (3a) with $\tilde{\mu}_a = 0$ yields a linear oscillator with frequency n for the absorber motion. Thus, the *global* steady state solution of the unperturbed system is simply a constant rotor speed, $y = 1$, and harmonic motion of each absorber with frequency n. This limiting case can be imagined as that with an enormous flywheel attached to the rotor, in which the absorbers move in a harmonic manner but have no rotor, which happily spins at a constant rate. In such a situation, the absorbers see a constant speed centrifugal field in which their undamped response is purely harmonic for all amplitudes up to the cusp point; this is the main point of using the tautochronic absorber path [7]. Note that in this limiting case the amplitudes of the absorbers' emotions are restricted, other than by the limit imposed by the cusps on the path. Then, since the rotor speed will change smoothly as the absorber mass, the applied torque, and the absorber damping are increased from zero, y will be smooth in ε and can be expanded as

$$y(\theta) = 1 + \varepsilon y_1(\theta) + \mathcal{O}(\varepsilon^2), \tag{11}$$

where y_1 captures the speed fluctuations induced by the net interaction of the applied torque, damping effects, and the torques induced by the motions of the absorbers. Note that condition (5) is assumed to maintain as ε is increased from zero, thereby keeping the mean rotational rate near $y = 1$.

The non-dimensionalized angular acceleration of the rotor, $\ddot{\theta}(t)/\Omega^2$, is given in terms of the variable $y(\theta)$ by $yy'(\theta)$. Since the primary design goal of the absorber system is to decrease the steady state rotor acceleration, an important measure of absorber performance is given by the peak value (that is, the infinity norm) of $yy'(\theta)$ during a steady state response; this quantity is denoted herein by $\|yy'\|_{ss}$. It will be convenient to have simple expressions for this acceleration, and these can be derived as follows. Since $\varepsilon \ll 1$, and y_1 is bounded, $y(\theta)$ oscillates about unity and is never zero. Therefore, equation (3a) can be divided through by y in order to obtain an expression for s_i'' in terms of s_i, s_i' and y. Substitution of this expression into equation (3b) and utilization of equation (4) gives an exact expression for $yy'(\theta)$:

$$yy'(\theta) = \left[1 + \frac{\nu}{N}\sum_{i=1}^{N} n^4 s_i^2\right]^{-1}\left[-\hat{\mu}_0 y + \Gamma_0 + \hat{\Gamma}_\theta \sin(n\theta) + \frac{\nu}{N}\sum_{i=1}^{N}\left(2n^2 s_i' s_i y^2 - \frac{\mathrm{d}g(s_i)}{\mathrm{d}s_i} s_i'^2 y^2 + n^2 + s_i g(s_i) y^2 + 2\hat{\mu}_a s_i' g(s_i) y\right)\right]. \tag{12}$$

Utilizing the definition $\varepsilon \equiv v$, the scalings in equation (10), the expansion in equation (11), and the condition (5), a series approximation for yy' in terms of ε can be obtained as follows:

$$yy'(\theta) = -\varepsilon\left\{\frac{1}{N}\sum_{j=1}^{N}\left(-2n^2 s_j s_j' - n^2 g(s_j)s_j + \frac{\mathrm{d}g(s_j)}{\mathrm{d}s_j}\, s_j'^2\right) - \tilde{\Gamma}_\theta \sin(n\theta)\right\} + \mathcal{O}(\varepsilon^2). \quad (13)$$

The above equation shows that the non-dimensionalized angular acceleration is of order ε, a result consistent with physical intuition from the limiting case as $\varepsilon \to 0$.

3. APPLICATION OF AVERAGING

3.1. PREPARATION OF THE EQUATIONS OF MOTION

The method of averaging is used to determine the dynamic response for $0 < \varepsilon \ll 1$. To obtain equations in the correct form for the application of averaging, some modifications of the equations of motion are carried out. This amounts to expressing the rotor dynamics in terms of the absorber dynamics in an ε-expansion, and then eliminating the rotor dynamics from the absorber equations of motion, yielding a set of coupled oscillators describing the absorber motions. First, based on the expansions in equations (11) and (13), one can show that y'/y is the same as yy' to leading order in ε. Then by dividing equation (3a) through by y, a modified equation describing the absorber dynamics is obtained, into which the ε-series approximation of y'/y is substituted. Expanding the result in terms of ε yields a set of weakly coupled, weakly non-linear oscillators for the absorber dynamics. These oscillators, in which the dynamics of the rotor has been eliminated to first order, are

$$s_i'' + n^2 s_i = \varepsilon f_i(s_1, \ldots, s_N, s_1', \ldots, s_N', \theta) + \mathcal{O}(\varepsilon^2), \qquad 1 \leqslant i \leqslant N, \quad (14)$$

where

$$f_i(s_1, \ldots, s_N, s_1', \ldots, s_N', \theta)$$

$$= -\tilde{\mu}_a s_i' + [s_i' + g(s_i)]\left[\frac{1}{N}\sum_{j=1}^{N}\left(-2n^2 s_j s_j' - n^2 g(s_j)s_j + \frac{\mathrm{d}g(s_j)}{\mathrm{d}s_j}\, s_j'^2\right) - \tilde{\Gamma}_\theta \sin(n\theta)\right].$$

3.1.1. *Remarks:*

(1) These equations are weakly coupled. The weak coupling arises due to the fact that the absorbers are not directly coupled in a physical sense, but only indirectly so through the rotor, and each absorber has only a small effect on the rotor due to its small relative inertia.

(2) The equations of motion are weakly non-linear, even though the amplitude of motion of the absorbers is not assumed to be small. The weak non-linearity is due to the epicycloidal path used for the absorbers, which renders a linear equation of motion valid for all feasible absorber amplitudes when the rotor speed is constant. Again, due to the smallness of the absorbers' inertias, the rotor speed is nearly constant and the presence of the absorbers, the applied torque and the absorber damping are pushed out to first nonlinear order.

(3) The symmetry $\mathbf{S}_N$ is evident in equation (14), as the absorbers appear in a completely interchangeable manner.

In reference [11], the method of averaging was employed to find a criterion that determines the point at which the unison motion becomes unstable. Therein, the following transformation to amplitude and phase variables was introduced:

$$s_i = a_i \cos(\phi_i - n\theta) \qquad \text{and} \qquad s_i' = n a_i \sin(\phi_i - n\theta), \qquad 1 \leqslant i \leqslant N, \tag{15}$$

where a_i and ϕ_i are slowly varying due to the form of equation (14). A first order averaging process was then carried out to capture the evolutions of a_i and ϕ_i, $1 \leqslant i \leqslant N$. The resulting averaged equations can be expressed in terms of the corresponding first order averaged quantities r_i and φ_i, $1 \leqslant i \leqslant N$, respectively (see Appendix A). However, this approach fails to characterize the post-bifurcation dynamics in a convenient form, since the averaged equations are highly non-linear and coupled in terms of the amplitudes and phases. Essentially, while it is possible to find the post-bifurcation solutions using numerical methods, it is not possible to predict the behavior of the post-bifurcation dynamics in terms of system parameters. To solve this problem, a linear co-ordinate transformation among absorber displacements is used herein that splits the dynamics into two invariant subspaces, representing the unison motion and its complement, respectively.† This transformation is given by

$$\xi_1 = \frac{1}{N}\sum_{j=1}^{N} s_j, \qquad \xi_i = \frac{1}{N}(s_1 - s_i) \qquad \text{for} \qquad 2 \leqslant i \leqslant N. \tag{16}$$

3.1.2. *Remarks:*

(1) This transformation enables one to separate the dynamics in the subspace of the unison mode **V** with attendant co-ordinate ξ_1, from the dynamics in the complement space **W** with co-ordinates ξ_i, $2 \leqslant i \leqslant N$. From the results in reference [11], it is known that when the unison response (in which the N absorbers undergo synchronous motion) bifurcates, $(N-1)$ eigenvalues of this system response, which correspond to the system dynamics in **W**, cross the imaginary axis. Therefore, to determine the post-bifurcation behavior, the dynamics in **W** must be analyzed.

(2) Note that for a response in which a group of p absorbers move in unison, with s_1 included in that group, there will be $(p-1)\xi_i$'s with zero amplitudes and $(N-p)\xi_i$'s with non-zero amplitude (for $2 \leqslant i \leqslant N$). Furthermore, if the remaining $(N-p)$ absorbers move together, the non-zero ξ_i's $(2 \leqslant i \leqslant N)$ will be equal to one another.

(3) Each $\xi_i (2 \leqslant i \leqslant N)$, is orthogonal to ξ_1 but they are not orthogonal to one another. A standard *block diagonalization* technique (see reference [15]) suggests that one chooses a set of orthogonal co-ordinates to characterize the dynamics in **W** in order to find the linearized solutions near the bifurcation point. In contrast, herein the special transformation (16) is chosen for convenience in estimating the feasible operating range of the applied torque.

(4) The inverse of the transformation exists and is given by

$$s_1 = \sum_{j=1}^{N} \xi_j, \qquad s_i = \sum_{j=1}^{N} \xi_j - N\xi_i, \qquad \text{for} \qquad 2 \leqslant i \leqslant N. \tag{17}$$

(5) For efficiency of presentation, the matrix **T** is defined such that $\mathbf{s} = \mathbf{T}\boldsymbol{\xi}$ where $\mathbf{s} = [s_1, s_2, \ldots, s_N]^{\mathrm{T}}$ and $\boldsymbol{\xi} = [\xi_1, \xi_2, \ldots, \xi_N]^{\mathrm{T}}$.

† A similar transformation was used in [14] in order to put linearized equations in a useful form.

The final form for averaging is obtained by applying transformation (17) to the equations of the motion (14) and implementing a transformation to polar co-ordinates. First, substituting transformation (17) into equations (14) yields the following transformed equations of motion:

$$\xi_1'' + n^2\xi_1 = \varepsilon\hat{f}_1(\boldsymbol{\xi}, \boldsymbol{\xi}', \theta) + \mathcal{O}(\varepsilon^2), \qquad \xi_i'' + n^2\xi_i = \varepsilon\hat{f}_i(\boldsymbol{\xi}, \boldsymbol{\xi}', \theta) + \mathcal{O}(\varepsilon^2), \qquad 2 \leqslant i \leqslant N, \quad (18)$$

where

$$\hat{f}_1(\boldsymbol{\xi}, \boldsymbol{\xi}', \theta) = -\tilde{\mu}_a\xi_1' + \xi_1' Y(\mathbf{T}\boldsymbol{\xi}, \theta) + \frac{1}{N}\left[g\left(\sum_{j=1}^{N} \xi_j\right) + \sum_{i=2}^{N} g\left(\sum_{j=1}^{N} \xi_j - N\xi_i\right)\right] Y(\mathbf{T}\boldsymbol{\xi}, \theta),$$

$$\hat{f}_i(\boldsymbol{\xi}, \boldsymbol{\xi}', \theta) = -\tilde{\mu}_a\xi_i' + \xi_i' Y(\mathbf{T}\boldsymbol{\xi}, \theta) + \frac{1}{N}\left[g\left(\sum_{j=1}^{N} \xi_j\right) - g\left(\sum_{j=1}^{N} \xi_j - N\xi_i\right)\right] Y(\mathbf{T}\boldsymbol{\xi}, \theta),$$

$$2 \leqslant i \leqslant N,$$

$$Y(\mathbf{s}, \theta) = \frac{1}{N}\sum_{j=1}^{N} (-2n^2 s_j s_j' - n^2 g(s_j)s_j + (\mathrm{d}g(s_j)/\mathrm{d}s_j)s_j'^2) - \tilde{\Gamma}_\theta \sin(n\theta).$$

The polar transformation is then given by

$$\xi_i = \rho_i \cos(\psi_i - n\theta) \qquad \text{and} \qquad \xi_i' = n\rho_i(\psi_i - n\theta), \qquad 1 \leqslant i \leqslant N. \quad (19)$$

Note that this transformation is singular when ξ_i is zero, and it is therefore not appropriate for determining the stability of the unison mode. However, of interest here are the system dynamics in the post-bifurcation stage. Substituting transformation (19) into equations (18) results in a set of first order differential equations which describe the dynamics of ρ_i and ψ_i, $1 \leqslant i \leqslant N$:

$$\rho_i' = (\varepsilon/n)\hat{F}_i(\rho_1, \ldots, \rho_N, \psi_1, \ldots, \psi_N, \theta)\sin(\psi_i - n\theta) + \mathcal{O}(\varepsilon^2), \quad (20a)$$

$$\rho_i\psi_i' = (\varepsilon/n)\hat{F}_i(\rho_1, \ldots, \rho_N, \psi_1, \ldots, \psi_N, \theta)\cos(\psi_i - n\theta) + \mathcal{O}(\varepsilon^2), \qquad 1 \leqslant i \leqslant N, \quad (20b)$$

where the function $\hat{F}_i$ is simply $\hat{f}_i$ expressed in terms of co-ordinates ρ_i and ψ_i, as obtained by incorporating transformation (19) into $\hat{f}_i$. It should be pointed out at this stage that in terms of the co-ordinates ρ_i's and ψ_i's, the subspace of the unison mode $\mathbf{V}$ is spanned by $[\rho_1, \psi_1, 0, 0, \ldots, 0, 0]^{\mathrm{T}}$ and the complement $\mathbf{W}$ is spanned by $[0, 0, \rho_2, \psi_2, \ldots, \rho_N, \psi_N]^{\mathrm{T}}$. Equations (20a) and (20b) are in the desired form for averaging.

3.2. THE AVERAGED EQUATIONS

Considering only the first order terms in ε in equations (20a) and (20b), averaging is performed in θ over one period of the excitation, $2\pi/n$. The resulting averaged equations are expressed in terms of the first order averaged variables $\bar{\rho}_i$ and $\bar{\psi}_i$, $1 \leqslant i \leqslant N$. Due to the complicated nature of the system, this process results in many terms in the forms of integrals, which render closed form solutions unachievable.

In order to obtain simplified, approximate estimates of the rotor acceleration and the operating torque range, it is assumed that the oscillation amplitudes of the absorbers, that is, the $\bar{\rho}_i$'s, are small and of the same order, denoted $\mathcal{O}(\bar{\rho})$. Then the averaged equations can be expanded in terms of the $\bar{\rho}_i$'s. This yields a set of truncated, averaged equations

in terms of $\bar{\rho}_i$ and $\overline{\psi}_i$, $1 \leqslant i \leqslant N$, as follows, where each is expanded to the desired order (more on this below):

$$\frac{\mathrm{d}\bar{\rho}_1}{\mathrm{d}\hat{\theta}} = \frac{-\tilde{\mu}_a\bar{\rho}_1}{2} + \frac{\tilde{\Gamma}_\theta}{2n}\cos\overline{\psi}_1 + \mathcal{O}(\bar{\rho}^3), \qquad \bar{\rho}_1\frac{\mathrm{d}\overline{\psi}_1}{\mathrm{d}\hat{\theta}} = -\frac{\tilde{\Gamma}_\theta}{2n}\sin\overline{\psi}_1 - \frac{n\bar{\rho}_1}{2} + \mathcal{O}(\bar{\rho}^3), \quad \text{(21a, b)}$$

$$\begin{aligned}\frac{\mathrm{d}\bar{\rho}_i}{\mathrm{d}\theta} = {} & \frac{-\tilde{\mu}_a\bar{\rho}_i}{2} + \frac{n^3}{4}\bar{\rho}_1^2\bar{\rho}_i\sin(2\overline{\psi}_1 - 2\overline{\psi}_i) \\ & + \frac{n^3\bar{\rho}_i}{4}\sum_{j\neq 1,i}\{2\bar{\rho}_i\bar{\rho}_j\sin(\overline{\psi}_i - \overline{\psi}_j) - (N-1)\bar{\rho}_j^2\sin[2(\overline{\psi}_i - \overline{\psi}_j)]\} \\ & + \frac{n^3\bar{\rho}_i}{2}\sum_{j,k\neq 1,i \text{ and } j\neq k}\bar{\rho}_j\bar{\rho}_k\sin(2\overline{\psi}_i - \overline{\psi}_j - \overline{\psi}_k) \\ & + \frac{(n^2+n^4)\bar{\rho}_i}{16n}\left\{N\tilde{\Gamma}_\theta\bar{\rho}_i\cos\psi_i - \sum_{j=1}^{N}2\tilde{\Gamma}_\theta\bar{\rho}_j\cos(2\overline{\psi}_i - \overline{\psi}_j)Nn^2\bar{\rho}_1\bar{\rho}_i\sin(\overline{\psi}_1 - \overline{\psi}_i)\right. \\ & \left. - \sum_{j=1}^{N}2n^2\bar{\rho}_1\bar{\rho}_j\sin(\overline{\psi}_1 - 2\overline{\psi}_i + \overline{\psi}_j)\right\} + \mathcal{O}(\bar{\rho}^5), \end{aligned} \quad \text{(21c)}$$

$$\begin{aligned}\bar{\rho}_i\frac{\mathrm{d}\overline{\psi}_i}{\mathrm{d}\hat{\theta}} = {} & -\frac{n^3}{4}\bar{\rho}_i\bar{\rho}_1^2\cos(2\overline{\psi}_1 - 2\overline{\psi}_i) - \frac{(N-1)}{4}n^3\bar{\rho}_i^3 \\ & + \frac{n^3\bar{\rho}_i}{4}\sum_{j\neq 1,i}\{2\bar{\rho}_i\bar{\rho}_j\cos(\overline{\psi}_i - \overline{\psi}_j) - (N-1)\bar{\rho}_j^2\cos[2(\overline{\psi}_i - \overline{\psi}_j)]\} \\ & + \frac{n^3\bar{\rho}_i}{2}\sum_{j,k\neq 1,i \text{ and } j\neq k}\bar{\rho}_j\bar{\rho}_k\cos(2\overline{\psi}_i - \overline{\psi}_j - \overline{\psi}_k) \\ & + \frac{(n^2+n^4)\bar{\rho}_i}{16n}\left\{-3N\tilde{\Gamma}_\theta\bar{\rho}_i\sin\psi_i + \sum_{j=1}^{N}[2\tilde{\Gamma}_\theta\bar{\rho}_j\sin(2\overline{\psi}_i - \overline{\psi}_j)\right. \\ & + 4\tilde{\Gamma}_\theta\bar{\rho}_j\sin\overline{\psi}_j] - 3Nn^2\bar{\rho}_1\bar{\rho}_i\cos(\overline{\psi}_i - \overline{\psi}_1) \\ & \left. + \sum_{j=1}^{N}[2n^2\bar{\rho}_1\bar{\rho}_j\cos(2\overline{\psi}_i - \overline{\psi}_1 - \overline{\psi}_j) + 4n^2\bar{\rho}_1\bar{\rho}_j\cos(\overline{\psi}_1 - \overline{\psi}_j)]\right\} + \mathcal{O}(\bar{\rho}^5), \end{aligned} \quad \text{(21d)}$$

where $2 \leqslant i \leqslant N$ and $\hat{\theta} \equiv \varepsilon\theta$.

3.3. STEADY STATE RESPONSES

Note that equations (21c) and (21d) are expanded out to third order, while terms out to fifth order are retained in the remaining equations. This is consistent for obtaining steady state solutions, as the $\mathcal{O}(\bar{\rho}^3)$ terms in the dynamics of $\bar{\rho}_1$ and $\overline{\psi}_1$ contribute at $\mathcal{O}(\bar{\rho}^5)$ in the dynamics of $\bar{\rho}_i$ and $\overline{\psi}_i$, $2 \leqslant i \leqslant N$. Since only the first order non-linear terms in the dynamics of $\bar{\rho}_i$ and $\overline{\psi}_i$, $2 \leqslant i \leqslant N$, are needed to find the desired approximate solutions, the $\mathcal{O}(\bar{\rho}^3)$ terms in $\bar{\rho}_1$ and $\overline{\psi}_1$ are not needed. This fact implies that only the linear dynamics of the unison response are needed in order to determine the first order non-linear steady

state solution of the non-unison component (this is most easily seen by making use of the proper co-ordinates, as done here). In the above suggested method for finding the approximate solutions, it is assumed that the $\mathcal{O}(\bar{\rho}^3)$ and $\mathcal{O}(\varepsilon)$ terms in averaged equations dominate the $\mathcal{O}(\varepsilon^2)$ terms resulting from the second order averaging (which is not considered here). The validity of this assumption depends on the actual values of ε and ρ which depend on the level of the disturbing torque. It will be shown in the simulations that the present expansion method provides satisfactory prediction for the system dynamics well beyond the bifurcation.

To find a simple approximation for the steady-state solution for $\bar{\rho}_1$ and $\bar{\psi}_1$, it is assumed that $\tilde{\mu}_a$ is small compared to n (this is true in most applications), and that the $\mathcal{O}(\bar{\rho}^3)$ terms in equations (21a) and (21b) are neglected. Setting equations (21a) and (21b) equal to zero yields the following approximate steady state solutions for $\bar{\rho}_1$ and $\bar{\psi}_1$, denoted by $\tilde{\bar{\rho}}_1$ and $\tilde{\bar{\psi}}_1$,

$$\tilde{\bar{\rho}}_1 = \tilde{\Gamma}_\theta / n^2 \qquad \text{and} \qquad \tilde{\bar{\psi}}_1 = -\pi/2. \tag{22}$$

This is nothing more than the linear undamped response, but a reasonable approximation of the unison mode at steady state, even up to amplitudes for which the bifurcation occurs; this is verified by simulations. Substituting the above solutions into equations (21c) and (21d), setting their derivatives equal to zero, and ignoring the $\mathcal{O}(\bar{\rho}^5)$ terms, a set of stationary equations obtains which can be solved for the approximate steady state solutions of $\bar{\rho}_i$ and $\bar{\psi}_i$, $2 \leqslant i \leqslant N$, denoted here as $\tilde{\bar{\rho}}_i$ and $\tilde{\bar{\psi}}_i$, respectively. These equations are

$$0 = \frac{-\tilde{\mu}_a \tilde{\bar{\rho}}_i}{2} + \frac{\tilde{\Gamma}_\theta^2 \tilde{\bar{\rho}}_i}{2} \sin(2\tilde{\bar{\psi}}_i) + \frac{n^3 \tilde{\bar{\rho}}_i}{4} \sum_{j \neq 1,i} \{2\tilde{\bar{\rho}}_i \tilde{\bar{\rho}}_j \sin(\tilde{\bar{\psi}}_i - \tilde{\bar{\psi}}_j) - (N-1)\tilde{\bar{\rho}}_j^2 \sin[2(\tilde{\bar{\psi}}_i - \tilde{\bar{\psi}}_j)]\} + \frac{n^3 \tilde{\bar{\rho}}_i}{2} \sum_{j,k \neq 1,i \text{ and } j \neq k} \tilde{\bar{\rho}}_j \tilde{\bar{\rho}}_k \sin(2\tilde{\bar{\psi}}_i - \tilde{\bar{\psi}}_j - \tilde{\bar{\psi}}_k), \tag{23a}$$

$$0 = \frac{\tilde{\Gamma}_\theta^2 \tilde{\bar{\rho}}_i}{4n} \cos(2\tilde{\bar{\psi}}_i) - \frac{(N-1)n^3}{4} \tilde{\bar{\rho}}_i^3 + \frac{n^3 \tilde{\bar{\rho}}_i}{4} \sum_{j \neq 1,i} \{2\tilde{\bar{\rho}}_i \tilde{\bar{\rho}}_j \cos(\tilde{\bar{\psi}}_i - \tilde{\bar{\psi}}_j) - (N-1)\tilde{\bar{\rho}}_j^2 \cos[2(\tilde{\bar{\psi}}_i - \tilde{\bar{\psi}}_j)]\} + \frac{n^3 \tilde{\bar{\rho}}_i}{2} \sum_{j,k \neq 1,i \text{ and } j \neq k} \tilde{\bar{\rho}}_j \tilde{\bar{\rho}}_k \cos(2\tilde{\bar{\psi}}_i - \tilde{\bar{\psi}}_j - \tilde{\bar{\psi}}_k), \qquad 2 \leqslant i \leqslant N. \tag{23b}$$

Note that up to this point, $(\bar{\cdot})$'s denote the first order averaged quantities of ρ's and ψ's and $(\tilde{\bar{\cdot}})$'s denote the associated truncated, steady state quantities of $(\bar{\cdot})$'s when the absorber damping is neglected in the unison mode. The post-bifurcation dynamics are investigated using the truncated equations in equations (21) and (23), as well as their non-truncated version in Appendix A. The first approach has the advantage of providing explicit results in terms of the system parameters, whereas the second approach is more accurate. (One should note that for simplicity the equations in Appendix A capture the system dynamics in terms of the s co-ordinates, which are different from the ξ co-ordinates used throughout this paper.)

4. THE POST-BIFURCATION DYNAMICS

In this section a first order approximation of the post-bifurcation dynamics is examined based on the truncated equations obtained in the previous section. Some general remarks, notational definitions and a brief overview of this section are provided before the detailed results are presented.

It is very difficult to determine all solution branches and their stabilities in a problem with this level of symmetry. However, for the problem at hand, it is possible to estimate certain important features of the response, including the angular acceleration of the rotor and the feasible torque range. Note that the torque range is imposed by the restriction stated in inequality (6), the constraint on the amplitude of the absorber motions. Therefore, an estimate for the peak amplitude over all absorber motions at the steady state, denoted by $\| s \|_{ss}$, is needed.

In section 4.1, it is first shown that all possible post-bifurcation, steady state solutions lie near the surface of an ellipsoid formed by the steady-state amplitudes of the $\tilde{\rho}_i$'s, $2 \leqslant i \leqslant N$. Some of the solutions on this ellipsoid are those with the corresponding isotropy subgroups, $\mathbf{S}_p \times \mathbf{S}_{N-p}$, for $1 < p < N$. For simplicity, such solutions are referred to as "an $\mathbf{S}_p \times \mathbf{S}_{N-p}$ solution", or "an $\mathbf{S}_p \times \mathbf{S}_{N-p}$ branch". A $\mathbf{S}_p \times \mathbf{S}_{N-p}$ solution simply refers to one with p absorbers moving in relative unison and the other $(N-p)$ absorbers also moving in relative unison, but with a different amplitude and/or phase than the first p.

In section 4.2., based on the results obtained in section 4.1., it is shown that among all the possible solution branches, the $\mathbf{S}_1 \times \mathbf{S}_{N-1}$ branch leads to the maximum $\|s\|_{ss}$ of all possible absorber motions. In section 4.3., one of the $\mathbf{S}_1 \times \mathbf{S}_{N-1}$ branches is proven to be dynamically stable, based on the truncated equations in the set (21). This information is then used in section 5 to estimate the feasible torque range.

4.1. APPROXIMATE POST-BIFURCATION SOLUTIONS

Based on equations (23), for each i there exist steady-state solutions with $\tilde{\rho}_i = 0$ or $\tilde{\rho}_i \neq 0$. As time goes to infinity, some of the $\tilde{\rho}_i$'s, $2 \leqslant i \leqslant N$, may converge to $\tilde{\rho}_i = 0$ while the others converge to non-zero steady state amplitudes, depending on initial conditions and the stabilities of the various solution branches. For simplicity, the following sets of indices are defined

$$\mathscr{Z} \equiv \left\{ i \mid \lim_{\theta \to \infty} \tilde{\rho}_i(\theta) = 0,\ 2 \leqslant i \leqslant N \right\}, \qquad \mathscr{N} \equiv \left\{ i \mid \lim_{\theta \to \infty} \tilde{\rho}_i(\theta) \neq 0,\ 2 \leqslant i \leqslant N \right\}, \tag{24}$$

which contain those indices corresponding to zero and non-zero steady state amplitudes, respectively. For those $\tilde{\rho}_i$ with i in $\mathscr{Z}$, the solution for the steady state phase $\tilde{\bar{\psi}}_i$ is arbitrary. For the remaining $\tilde{\rho}_i$, that is, those with i in $\mathscr{N}$, it can be assumed that the corresponding phases are identical; i.e., $\tilde{\bar{\psi}}_i = \tilde{\bar{\psi}}_j$, $\forall i,\ j \in \mathscr{N}$ (see Appendix B for a justification of this assumption.) Applying the results obtained to equations (23) yields an ellipsoid prescribed by

$$N \sum_{i=2}^{N} \tilde{\rho}_i^2 - \sum_{i=2}^{N} \sum_{j=2}^{N} \tilde{\rho}_i \tilde{\rho}_j = \left(\frac{\tilde{\Gamma}_\theta^4}{n^8} - \frac{4\tilde{\mu}_a^2}{n^6} \right)^{1/2} \tag{25}$$

such that the steady-state solutions of $\tilde{\rho}_i$, $i \in \mathscr{N}$ lie on this ellipsoid (as a first order approximation). The formulation of this ellipsoid is independent of number of the

non-zero steady state $\tilde{\rho}_i$'s, i.e., of the size of $\mathscr{N}$, but its dimension depends on the size of $\mathscr{N}$.

Note that the ellipsoid exists only for system and excitation parameters satisfying

$$\tilde{\Gamma}_\theta \geqslant \sqrt{2n\tilde{\mu}_a}, \tag{26}$$

which is equivalent to the simplified bifurcation criterion for the unison motion obtained in reference[11].

Note also that since this ellipsoid results from the truncated equations (23); when the non-truncated equations are considered the ellipsoid will be distorted or even disappear in the sense that only a finite number of points on the (distorted) ellipsoid will survive as legitimate steady state solutions.†

Some information about the nature of the solutions on the ellipsoid can be garnered from symmetric bifurcation theory. Consider a case in which p and $N-p$ groups of absorbers move in distinct, but relative unison motions. (Note that in this case $(p-1)$ is the size of $\mathscr{Z}$, since the first absorber is not included in $\mathscr{Z}$.) As for the other $\tilde{\rho}_i$, that is, the $N-p$ with $i \in \mathscr{N}$, their steady state solutions lie on the surface of the ellipsoid (25). Based on the "Equivariant Branching Lemma" proposed by Cicogna [16] and Vanderbauwhede [17], when certain conditions are satisfied,‡ the $\mathbf{S}_p \times \mathbf{S}_{N-p}$ solution branches generically exist for all p, $1 \leqslant p \leqslant N$. Therefore, the existence of the solution branches on the surface of the ellipsoid with identical amplitudes ρ_i and phases ψ_i for each $i \in \mathscr{N}$ is generically ensured for the non-truncated averaged equations. Attention is now turned to the most important of these solution branches. (Note that travelling wave types of solutions are also possible in the generic case, but these have not been observed for the system under consideration. They may not exist, or may be dynamically unstable for this system.)

4.2. SEARCH FOR THE SOLUTION BRANCH LEADING TO THE MAXIMUM $\|s\|_{ss}$

Instead of finding all possible solution branches, a search for the branch leading to the maximum $\|s\|_{ss}$ is conducted in order to estimate the feasible torque range. This is accomplished by substituting the polar form of the absorber responses given in equation (19) into the absorber displacements in terms of the ξ-co-ordinates given in equations (17), and assuming identical phases for each absorber during steady state operation (this is the assumption justified in Appendix B). From this, one can express the steady state peak value of the first absorber motion by

$$\|s_1\|_{ss} \equiv \max\{s_1(\theta) \mid \theta_0 \leqslant \theta \leqslant \theta_0 + 2\pi,\ \theta_0 \to \infty\}$$

$$\simeq \left[\left(\sum_{i=2}^{N} \tilde{\rho}_i\right)^2 - \frac{2\tilde{\Gamma}_\theta}{n^2} \sin(\tilde{\psi}_i)\left(\sum_{i=2}^{N} \tilde{\rho}_i\right) + \frac{\tilde{\Gamma}_\theta^2}{n^4}\right]^{1/2}, \tag{27}$$

which is a square root of a positive quadratic function of $\Sigma_{i=2}^{N} \tilde{\rho}_i$. (Note that it is implied from equations (23) and Appendix B that $\sin(\tilde{\psi}_i)$ is independent of $\tilde{\rho}_i$, $2 \leqslant i \leqslant N$.) Subject

† Working to first nonlinear order predicts the existence of this invariant ellipsoid, but it does not provide the dynamics on it. This could presumably be obtained by using higher order averaging. However, for present purposes this is not necessary.

‡ These two conditions are (also see reference [12]): (1) The symmetric group $\mathbf{S}_N$ acts on $\mathbf{W}$ irreducibly. (2) The critical eigenvalues cross the imaginary axis with non-zero speed as the parameter of interest is varied. These conditions can be verified in the present case. However, one still needs to prove that the present bifurcation problem is *generic*. It is not the authors' intention to complete such a rigorous proof in this paper. The "Equivariant Branching Lemma" is simply used as a road map to search for possible solution branches, and their existence can be confirmed by numerically solving the non-truncated averaged equations given in Appendix A.

to the ellipsoid in equation (25), $\|s_1\|_{ss}$ will reach its maximum value when $\Sigma_{i=2}^{N} \tilde{\rho}_i$ reaches its extremum. Since $\Sigma_{i=2}^{N} \tilde{\rho}_i = 0$ is a principal axis for the ellipsoid, $\Sigma_{i=2}^{N} \tilde{\rho}_i$ reaches its extrema at the direction of the associated eigenvector where $\tilde{\rho}_i = \tilde{\rho}_j$, $2 \leqslant i, j \leqslant N$. Hence, among all the possible post-bifurcation solutions, the one with identical $\tilde{\rho}_i$ and $\tilde{\bar{\psi}}_i$, $2 \leqslant i \leqslant N$, leads to the maximum $\|s_1\|_{ss}$. It can be easily shown that the maximum $\|s_i\|_{ss}$ for all $2 \leqslant i \leqslant N$ is equal to the maximum $\|s_1\|_{ss}$, since the results are preserved under different choices of the first absorber due to identity of all absorbers. As a result, among all the possible post-bifurcation solutions, the one with identical $\tilde{\rho}_i$ and $\tilde{\bar{\psi}}_i$ for $2 \leqslant i \leqslant N$ leads to the maximum $\|s\|_{ss}$ of all possible absorber motions on the steady state ellipsoid. This solution corresponds to the isotropy subgroup $\mathbf{S}_1 \times \mathbf{S}_{N-1}$ wherein one absorber moves out of step relative to all other absorbers, which remain in relative unison.

Based on the Equivariant Branching Lemma, at least one such solution branch is expected to exist. The Newton–Raphson method was employed to numerically determine from the non-truncated averaged equations (given in Appendix A) that such branches indeed exist in the post-bifurcation stage over a wide range of parameter values.

4.3. STABILITY OF THE $S_1 \times S_{N-1}$ SOLUTION BRANCH

With the existence of the $\mathbf{S}_1 \times \mathbf{S}_{N-1}$ solution in hand, a stability analysis is carried out based on the truncated equations (21).

Consider equations (21a) and (21b), in which $\bar{\rho}_1$ and $\bar{\psi}_1$ capture the dynamics of the unison mode. The steady state solutions of $\bar{\rho}_1$ and $\bar{\psi}_1$ can be approximated by

$$\bar{\rho}_1 = \hat{\bar{\rho}}_1 + \mathcal{O}(\bar{\rho}^3) \qquad \text{and} \qquad \tan \bar{\psi}_1 = \tan \hat{\bar{\psi}}_1 + \mathcal{O}(\bar{\rho}^3), \tag{28}$$

where

$$\hat{\bar{\rho}}_1 = \tilde{\Gamma}_\theta / n(\tilde{\mu}_a^2 + n^2)^{1/2}, \qquad \tan \hat{\bar{\psi}}_1 = -n/\tilde{\mu}_a, \tag{29}$$

which, when truncated, is simply the linear, damped steady state unison solution. Note that compared to the approximate solutions (22), here the effect of damping is required since it is crucial to the stability analysis of the $\mathbf{S}_1 \times \mathbf{S}_{N-1}$ branch.

This approximate solution is independent of $\bar{\rho}_i$ and $\bar{\psi}_i$, $2 \leqslant i \leqslant N$, up to $\mathcal{O}(\bar{\rho}^3)$ (that is, the unison dynamics are independent of the non-unison dynamics to second order). By treating the $\mathcal{O}(\bar{\rho}^3)$ terms as non-vanishing perturbations in equations (21a) and (21b), it can be shown (using Lyapunov techniques) that there exists a positive number Θ, independent of $\bar{\rho}_i(\theta)$, $\bar{\psi}_i(\theta)$, $2 \leqslant i \leqslant N$, such that $[\bar{\rho}_1(\theta), \bar{\psi}_1(\theta)]^{\mathrm{T}}$ is ultimately bounded in an $\mathcal{O}(\bar{\rho}^3)$ neighborhood of $[\hat{\bar{\rho}}_1(\theta), \hat{\bar{\psi}}_1(\theta)]^{\mathrm{T}}$ for $\theta \geqslant \Theta$. Hence, the stability of the $\mathbf{S}_1 \times \mathbf{S}_{N-1}$ branch can be examined by incorporating the approximate solution from equation (28) in equations (21c) and (21d), which govern the dynamics of $\bar{\rho}_i$, $\bar{\psi}_i$, $2 \leqslant i \leqslant N$, and in which the $\mathcal{O}(\bar{\rho}^3)$ terms in equations (28) only contribute to the terms of $\mathcal{O}(\bar{\rho}^5)$.

The subsystem consisting of equations (21c) and (21d), governing the dynamics of $\bar{\rho}_i$ and $\bar{\psi}_i$, $2 \leqslant i \leqslant N$, is considered for the stability analysis. The Jacobian of this system is first derived and evaluated on the $\mathbf{S}_1 \times \mathbf{S}_{N-1}$ branch. Due to the symmetry of the subsystem and this solution, this Jacobian, denoted by J, has the form

$$J_{(2N-2)\times(2N-2)} = \begin{bmatrix} A_{2\times 2} & B_{2\times 2} & \cdots & B_{2\times 2} \\ B_{2\times 2} & A_{2\times 2} & \cdots & B_{2\times 2} \\ \vdots & \vdots & \ddots & B_{2\times 2} \\ B_{2\times 2} & B_{2\times 2} & B_{2\times 2} & A_{2\times 2} \end{bmatrix}. \tag{30}$$

It can be shown that all eigenvalues of J are eigenvalues of one of the 2×2 matrices, $[\mathrm{A} + (N-2)\mathrm{B}]$ or $[\mathrm{A} - \mathrm{B}]$. This result is a consequence of the symmetry and does not

depend on the actual values of A and B. The nature of the eigenvalues of [A − B] are first determined by the well-known fact that both eigenvalues of a 2 × 2 matrix possess negative real parts if and only if the trace is negative and the determinant is positive. By incorporating equations (28) into the Jacobian J, the determinant and trace of [A − B] are determined to be

$$\text{Trace [A} - \text{B]} = -\tilde{\mu}_a, \tag{31a}$$

$$\begin{aligned}\text{Det [A} - \text{B]} = (N\tilde{\mu}_a(n^2 + n^4)/256)\hat{\bar{\rho}}\hat{\bar{\rho}}_1[(12 - 5N)(n^2 + n^4)\hat{\bar{\rho}}\hat{\bar{\rho}}_1 \\ + (4N - 12)(n^2 + n^4)\hat{\bar{\rho}}\hat{\bar{\rho}}_1 \cos(2\hat{\bar{\psi}} - 2\hat{\bar{\psi}}_1) + 16\cos(\hat{\bar{\psi}} - \hat{\bar{\psi}}_1)] + \mathcal{O}(\bar{\rho}^6),\end{aligned} \tag{31b}$$

where $\hat{\bar{\rho}}$ and $\hat{\bar{\psi}}$ are used to denote the steady state amplitudes and phases of $\bar{\rho}_i$ and $\bar{\psi}_i$, $2 \leqslant i \leqslant N$, respectively, on the $\mathbf{S}_1 \times \mathbf{S}_{N-1}$ branch. Since the trace is always negative, only the sign of Det [A − B] needs to be determined. Letting $\hat{\bar{\rho}} \to 0^+$, it is found that the sign of Det [A − B] is dominated by the sign of $\cos(\hat{\bar{\psi}} - \hat{\bar{\psi}}_1)$ near the bifurcation point. Based on equations (23), near the bifurcation point,

$$\hat{\bar{\psi}} \simeq -3\pi/4 \qquad \text{or} \qquad \pi/4. \tag{32}$$

The above two solutions for the phases provide two different $\mathbf{S}_1 \times \mathbf{S}_{N-1}$ solution branches. With the approximate value of ψ_1 given in equation (22), one has

$$\cos(\hat{\bar{\psi}} - \hat{\bar{\psi}}_1) \simeq \begin{cases} 1/\sqrt{2}, & \text{for } \hat{\bar{\psi}} \simeq -3\pi/4, \\ -1/\sqrt{2}, & \text{for } \hat{\bar{\psi}} \simeq \pi/4, \end{cases}$$

near the bifurcation point. The first branch, with $\hat{\bar{\psi}} \simeq -3\pi/4$, leads to Det [A − B] > 0 as $\hat{\bar{\rho}} \to 0^+$ while the other branch similarly leads to Det [A − B] < 0.

As for the [A + (N − 2)B] matrix, in Appendix C it is proved that the branch with $\hat{\bar{\psi}} \simeq -3\pi/4$ leads to Trace [A + (N − 2)B] < 0 and Det [A + (N − 2)B] > 0 as $\hat{\bar{\rho}} \to 0^+$ near the bifurcation point. Hence, the $\mathbf{S}_1 \times \mathbf{S}_{N-1}$ branch with $\hat{\bar{\psi}}$ close to $-3\pi/4$ is stable. Henceforth, this branch will be designated as "the stable $\mathbf{S}_1 \times \mathbf{S}_{N-1}$ branch".

5. ABSORBER PERFORMANCE

In this section, two important measures of absorber performance, the feasible operating range of the applied torque and the angular acceleration of the rotor, are estimated.

5.1. ESTIMATE OF THE FEASIBLE TORQUE RANGE

As the amplitude of the applied torque is increased, the absorbers' amplitudes likewise increase, until a cusp limit (6) is reached for one or more absorbers. Therefore, the feasible torque range can be determined if one combines the relationship between the torque amplitude and $\|s\|_{ss}$ with the absorber amplitude limit. This process is described here for both the truncated and non-truncated versions of the equations.

From the analytical results obtained in the previous section, it is known that there exists a stable $\mathbf{S}_1 \times \mathbf{S}_{N-1}$ solution which yields the maximum $\|s\|_{ss}$ (based on the truncated equations). This implies that for any initial conditions, the system will converge to a solution branch that renders an $\|s\|_{ss}$ which is less than or equal to that resulting from the stable $\mathbf{S}_1 \times \mathbf{S}_{N-1}$ branch. Therefore, this solution branch can be used to predict the maximum $\|s\|_{ss}$, which is used in turn to determine the feasible torque range.

By using the fact that the steady state amplitudes, ρ_i, $2 \leqslant i \leqslant N$, are all equal on the

stable $\mathbf{S}_1 \times \mathbf{S}_{N-1}$ solution branch, the ellipsoid prescribed in equation (25) can be used to determine the steady state amplitudes, yielding

$$\tilde{\rho} \equiv \tilde{\rho}_i = (1/\sqrt{N-1}(\tilde{\Gamma}_\theta^4/n^8 - 4\tilde{\mu}_a^2/n^6)^{1/4}, \qquad 2 \leqslant i \leqslant N. \tag{33}$$

Similarly, by using equations (23), the equal steady state phase on this solution branch are found to be

$$\tilde{\psi} \equiv \tilde{\psi}_i = \tfrac{1}{2}[\sin^{-1}(2n\tilde{\mu}_a/\tilde{\Gamma}_\theta^2)] - \pi, \qquad 2 \leqslant i \leqslant N. \tag{34}$$

It has been shown that $\|s\|_{ss}$ can be derived from $\|s_1\|_{ss}$. To determine $\|s_1\|_{ss}$, the expression for s_1 in terms of ξ_i, $1 \leqslant i \leqslant N$, given in equation (17), is utilized. Substituting the angular transformation (19) into this expression, using the stable $\mathbf{S}_1 \times \mathbf{S}_{N-1}$ branch and the approximate steady state unison solution for ρ_1 and ψ_1 given in equations (22), one obtains $\|s\|_{ss}$, as follows:

$$\|s\|_{ss} \equiv \max_{1 \leqslant i \leqslant N} \{s_i(\theta) \mid \theta_0 \leqslant \theta \leqslant (\theta_0 + 2\pi), \theta_0 \to \infty\}$$
$$\simeq [\tilde{\Gamma}_\theta^2/n^4 - 2/n^2(N-1)\tilde{\Gamma}_\theta\tilde{\rho}\sin\tilde{\psi} + (N-1)^2\tilde{\rho}^2]^{1/2}, \tag{35}$$

where $\tilde{\rho}$ and $\tilde{\psi}$ are given by equations (33) and (34), respectively.

It is now possible to estimate the feasible operating range of the applied torque level $\hat{\Gamma}_\theta$ by recalling inequality (6) and using the approximate expression for $\|s\|_{ss}$ in equation (35). This can be carried out to an analytical equation, which is not presented here since it is not easily solved for an explicit expression for the maximum torque. Note that since this estimate is based on the truncated equations in equation (23), it will deteriorate near the singularity of the absorber path. In order to determine a more accurate estimate for the torque range, one can numerically solve the non-truncated equations (A1a) and (A1b) (as described in Appendix A) for a more accurate estimate of the $\mathbf{S}_1 \times \mathbf{S}_{N-1}$ solution.

5.2. ESTIMATE OF THE ROTOR ACCELERATION

An approximate expression for the angular acceleration is first formulated to leading non-linear order, after which more accurate estimates are computed. Taking the non-dimensionalized acceleration $yy'(\theta)$ stated in the equation (13), considering only the $\mathcal{O}(\varepsilon)$ terms in $yy'(\theta)$, expanding $yy'(\theta)$ in terms of s_i, $1 \leqslant i \leqslant N$, and then using the definition $\varepsilon \equiv v$ and the transformation (16), yields

$$yy'(\theta) = v\left[\frac{2n^2}{N}\sum_{j=1}^{N} s_j s_j' + n^2\xi_1 + \tilde{\Gamma}_\theta \sin(n\theta)\right] + \mathcal{O}(\rho^3), \tag{36}$$

where only the first and second order amplitude terms are considered. Utilizing the truncated stationary equations (23), a non-trivial calculation (outlined in Appendix D) yields the following lower order approximation for $yy'(\theta)$,

$$yy'(\theta) \simeq \begin{cases} \varepsilon[n^3\tilde{\rho}_1^2 \sin(2\tilde{\psi}_1 - 2n\theta)] = (\hat{\Gamma}_\theta^2/vn)\sin(2n\theta), & \text{before bifurcation,} \\ \varepsilon[2\tilde{\mu}_a \cos(2\tilde{\psi} - 2n\theta)] = 2\hat{\mu}_a \cos(2\tilde{\psi} - 2n\theta), & \text{after bifurcation,} \end{cases} \tag{37}$$

where the approximate solution for $\tilde{\rho}_1$ and $\tilde{\psi}_1$ in equations (22) have been used and where

$$\tilde{\psi} = \tfrac{1}{2}\left[\sin^{-1}\left(\frac{2nv\hat{\mu}_a}{\hat{\Gamma}_\theta^2}\right)\right] - \pi.$$

An interesting feature of this result is that the peak value of $yy'(\theta)$; i.e., $\|yy'\|_{ss}$, is quadratic in terms of the applied torque level in the pre-bifurcation stage—this is due to the fact that the absorber is tuned to eliminate the acceleration at linear order. An even more interesting result is that in the post-bifurcation stage, $\|yy'\|_{ss}$ is independent of the torque level; i.e., it saturates after bifurcation. Furthermore, the acceleration $yy'(\theta)$ vanishes as $\hat{\mu}_a$ goes to zero. (Recall that the bifurcation torque level also goes to zero as $\hat{\mu}_a$ goes to zero.) Since the acceleration predicted by equations (37) saturates after bifurcation, higher order terms in ρ will become dominant when the applied torque level goes beyond the bifurcation level. In order to obtain a more accurate estimate, one can use the acceleration approximated to the next order, which is given by

$$yy'(\theta) \simeq v\left[\frac{2n^2}{N}\sum_{j=1}^{N} s_j s_j' + n^2\xi_1 + \tilde{\Gamma}_\theta \sin(n\theta) + (n^2+n^4)\sum_{j=1}^{N} s_j s_j'^2 - \frac{n^2(n^2+n^4)}{2}\sum_{j=1}^{N} s_j^3\right], \quad (38)$$

where s_i, $1 \leqslant i \leqslant N$ are approximated by equations (22), (33) and (34).

An even more accurate estimate can be obtained by numerically solving the non-truncated equations (A1a) and (A1b) given in Appendix A for the stable $\mathbf{S}_1 \times \mathbf{S}_{N-1}$ branch and substituting the resulting s_i, $1 \leqslant i \leqslant N$, into equation (13). These results are found to match simulations very closely over the entire feasible torque range.

6. NUMERICAL AND SIMULATION RESULTS

In this section, existence and stability results for steady state solutions are presented, along with simulation results, which are used to confirm the analytical results and to examine the accuracy of the various levels of approximations used in this study. In addition to the approximate results obtained in the previous sections, included here are numerical solutions of the non-truncated averaged equations (A1a) and (A1b) given in Appendix A. The system parameters used throughout this section are: $v = 0{\cdot}1662$ and $n = 2$; these were taken from the 2·5 l, in-line, four cylinder, four-stroke engine considered by Denman [7]. Recall that the authors' approximations are based on a small v assumption; the value considered here is a relatively large ratio for absorber systems, as typical values are often in the range 0·05–0·1. The absorber damping $\hat{\mu}_a$ is taken to be independent of the number of the absorbers, N [14].

The Newton–Raphson method was employed to solve the non-truncated averaged equations (A1a) and (A1b) for the post-bifurcation branches. This process was repeated for the following parameter ranges: $N = 2$–10 with increments of one, $\hat{\mu}_a = 0{\cdot}0013$–$0{\cdot}013$ with increments of 0·0001, $\hat{\Gamma}_\theta^* = 0{\cdot}03$–$0{\cdot}08$ with increments of 0·0001. In order to determine as many solutions as possible, several starting points were randomly chosen in the range $r_i = 0$–$0{\cdot}22$ (the cusp level) and $\varphi_i = 0$–2π, for each i. The associated stability of each solution was determined by numerically evaluating the eigenvalues of the associated Jacobian matrix. Numerical and simulation studies of many $\mathbf{S}_p \times \mathbf{S}_{N-p}$ solutions were carried out. It was found that in the post-bifurcation stage, for absorber amplitudes below the cusp level, the only stable solution branch is the $\mathbf{S}_1 \times \mathbf{S}_{N-1}$ branch considered in the analysis.

Equations (3a), (3b) and (4) were used to simulate directly the system dynamics, using Gear's BDF method [18]. It was found that by utilizing a wide range of initial conditions and the ranges of system parameters described above, the system dynamics always converged to the stable $\mathbf{S}_1 \times \mathbf{S}_{N-1}$ response in the post-bifurcation parameter range.

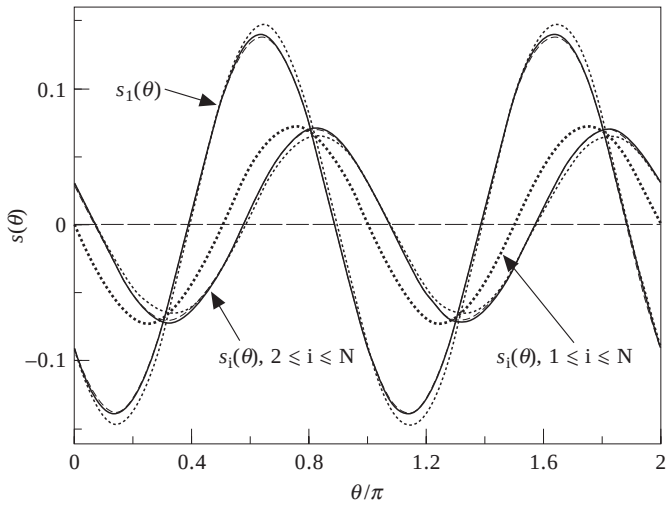

Figure 2. Post-bifurcation steady-state responses of the absorbers for $N = 4$ (four absorbers), $\hat{\mu}_a = 0{\cdot}0026$ and $\hat{\Gamma}_\theta = 0{\cdot}048$. ——, simulation; · · · · , truncated; - - - -, non-truncated; • • • • , imposed unison response.

Figure 2 shows a typical set of post-bifurcation absorber responses for $N = 4$, $\hat{\mu}_a = 0{\cdot}0026$ and $\hat{\Gamma}_\theta = 0{\cdot}048$. (Note that different values of $\hat{\mu}_a$ show qualitatively the same system dynamics as the value chosen here, although for higher damping levels the bifurcation of the unison response occurs nearer the cusp point.) In Figure 2, the solid lines represent the simulated response. The dotted lines are derived by estimating the response by truncated equations (22), (33), (34) and transformations (17). The dashed lines are obtained by assuming the stable $\mathbf{S}_1 \times \mathbf{S}_{N-1}$ solution ($= \mathbf{S}_1 \times \mathbf{S}_3$ here) and numerically solving the non-truncated averaged equations (A1a) and (A1b) for the absorber responses. The coarse dotted lines represent the simulated absorbers' responses if they are locked into a unison motion (that is, the absorber inertia is a single lumped mass). This shows that the non-truncated equations are very accurate and that the truncated equations are quite satisfactory. Note that the system response, as compared with the corresponding unison motion, has $N - 1(=3)$ absorbers with a slight phase shift and little amplitude difference, while one absorber undergoes a motion with drastically different amplitude and phase. It is the localized response of this absorber that will limit the applied torque range. (In the present analysis initial conditions will determine which absorber goes to the large amplitude, as any one is capable of doing so. In practice, small symmetry breaking discrepancies will favor localization in one of the absorbers.)

Figure 3 shows various estimates and simulations of the rotor acceleration for the same case as Figure 2. The second order approximation is derived by the truncated equations and the estimate given in equation (37), while the third order approximation is derived by the truncated equations and the estimate given in equation (38). It is seen that the second order approximation roughly represents the main harmonic component of the simulated acceleration but offers a poor prediction for $\|yy'\|_{ss}$. This is due to the fact that in the post-bifurcation stage, the terms up to $\mathcal{O}(\rho^2)$ in equation (13) saturate and the higher order harmonics begin to dominate $\|yy'\|_{ss}$. One remedy to this problem is to use the third order approximation, from equation (38), to estimate $\|yy'\|_{ss}$, which offers a significant improvement over the second order results. As expected, the non-truncated solution is in excellent agreement with the simulated acceleration in all regards.

Figure 4 shows $\|s\|_{ss}$ versus the applied torque level. The maximum amplitude, which

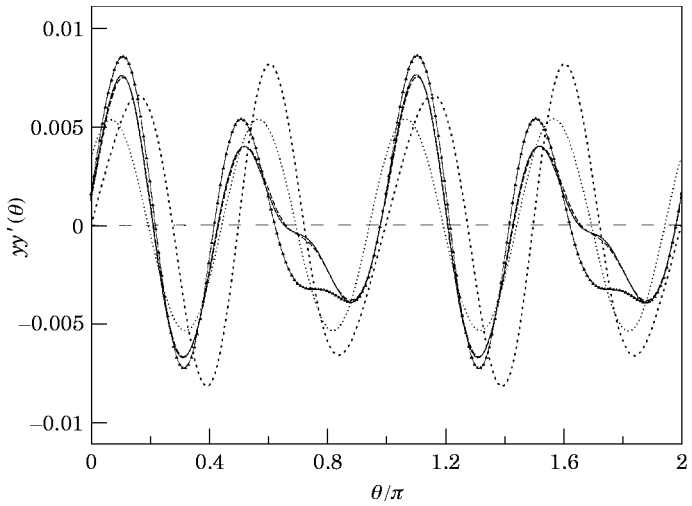

Figure 3. Post-bifurcation steady-state responses of the rotor acceleration for $N = 4$ (four absorbers), $\hat{\mu}_a = 0{\cdot}0026$ and $\hat{\Gamma}_\theta = 0.048$. ——, simulation; · · · ·, the 2nd-order approximation; ▲, the 3rd-order approximation; - - - -, non-truncated; · · · ·, imposed unison response.

fixes the range of the applied torque, is set by the restriction in equation (6) and is marked as "Cusp" in the figure.

From this figure, one observes that the truncated equations give a conservative prediction of the feasible torque range while the non-truncated equations give a very accurate estimate. Also, by comparing the unison and non-unison $\|s\|_{ss}$'s, one can see that the distribution of the total absorber mass into several smaller masses significantly decreases the operating torque range. Figure 5 shows the percent reduction in this range relative to the unison response for different numbers of absorbers. It is seen that as N increases, the feasible range is dramatically decreased by the bifurcation.

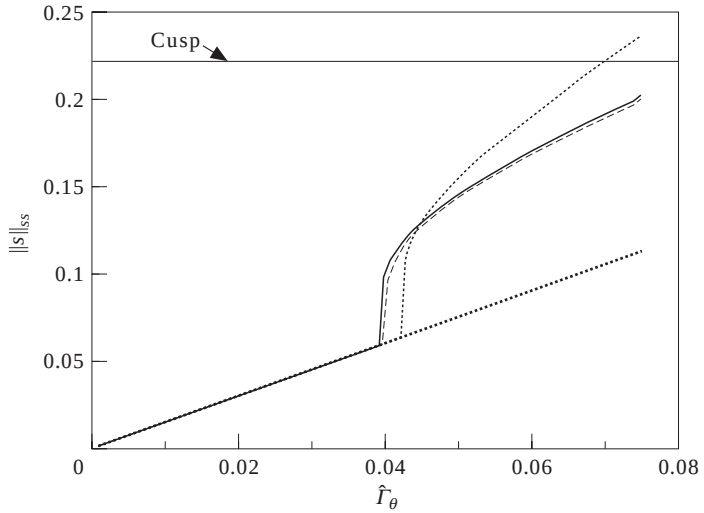

Figure 4. $\|s\|_{ss}$ derived by different approximations versus the applied torque level. The system parameters used are $N = 4$ and $\hat{\mu}_a = 0{\cdot}0026$. ——, simulation; · · · ·, truncated; - - - -, non-truncated; · · · ·, imposed unison response.

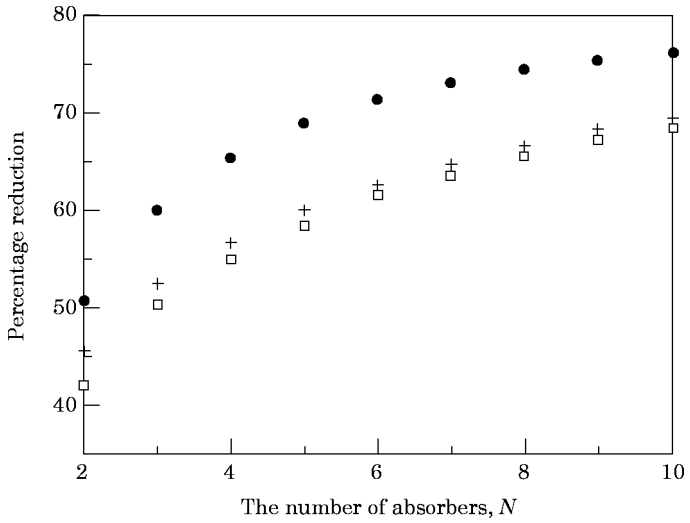

Figure 5. The percent reduction in torque range, relative to the unison motion, versus the number of absorbers for $\hat{\mu}_a = 0{\cdot}0026$. +, simulation; ●, truncated; □, non-truncated.

Figure 6 shows $\|yy'\|_{ss}$ versus the applied torque level. In this figure, the second order approximation completely saturates after the bifurcation, which is not observed in the simulations. The third order results are much improved, and the non-truncated equations again give a very accurate result. By comparing the $\|yy'\|_{ss}$'s for the unison and non-unison responses in the post-bifurcation range, one can see that the distribution of absorber mass slightly improves absorber system performance by decreasing the $\|yy'\|_{ss}$'s. Figure 7 shows the ratios of $\|yy'\|_{ss}$ to that for the unison response for various numbers of absorbers with $\hat{\Gamma}_\theta = 0{\cdot}0555$ and $\hat{\mu}_a = 0{\cdot}0026$. It is seen that the $\|yy'\|_{ss}$'s obtained from simulations are well approximated by the non-truncated equations. However, the second and third order results

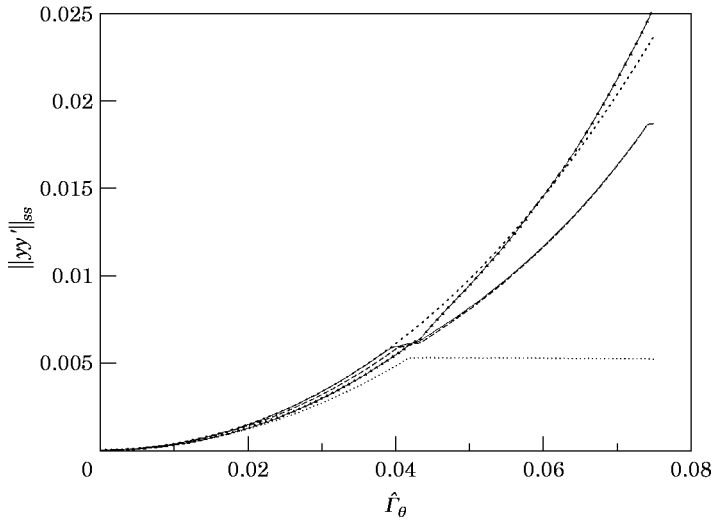

Figure 6. $\|yy'\|_{ss}$ derived by different approximations versus the applied torque level, for system parameters $N = 4$ and $\hat{\mu}_a = 0{\cdot}0026$. ——, simulation; · · · ·, the second order approximation; ▲, the third order approximation; - - - -, non-truncated; · · · ·, imposed unison response.

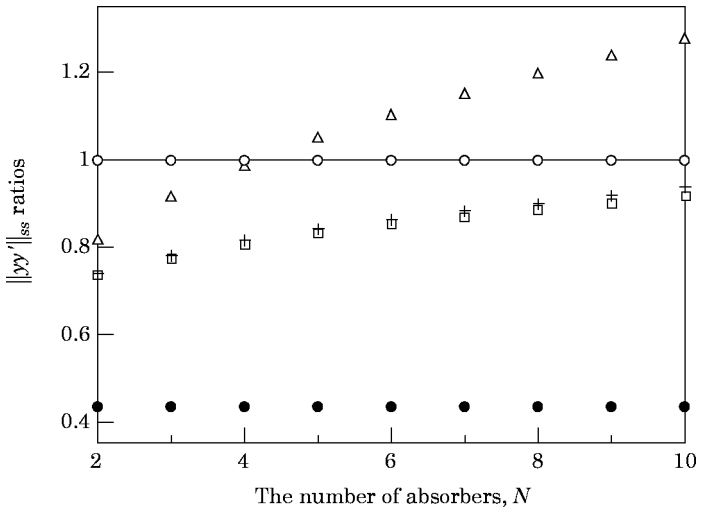

Figure 7. The ratio of $\|yy'\|_{ss}$ to that for the unison response versus the number of absorbers for $\hat{\Gamma}_\theta = 0{\cdot}0555$ and $\hat{\mu}_a = 0{\cdot}0026$. +, simulation; ●, second order approximation; △, third order approximation; □, non-trucated; ○, imposed unison response.

significantly under and over estimate this ratio, respectively. Also, it is seen that the actual ratio approaches unity as N increases.

Combining the results shown in Figures 5 and 7 indicates that one does not gain a significant reduction in the level of torsional oscillations by distributing the absorber mass, but the feasible torque range is drastically reduced.

7. CONCLUSIONS AND FUTURE WORK

This study considered the dynamic effects of using several masses to compose the required inertia for a system of tuned absorbers. For usual sizing calculations, one implicitly assumes that these masses move in a unison manner. In a previous study it was determined that this motion can become dynamically unstable as the torque level is increased [11]. In the present work the post-bifurcation dynamics are investigated. The results were obtained and verified by employing three methods: (1) low order truncations of the averaged equations, (2) numerically solving the non-truncated averaged equations, and (3) simulations. The truncated equations offer reliable qualitative results in terms of the dependence on system parameters, but are not very accurate in some respects. In contrast, the non-truncated results, while requiring numerical solutions of the steady-state equations, are very accurate in all respects.

It was found that the post-bifurcation dynamics are dominated by a stable $\mathbf{S}_1 \times \mathbf{S}_{N-1}$ steady-state solution branch. This is very reminiscent of *mode localization*, in that one absorber undergoes a much larger amplitude of motion relative to the others (see reference [19] for relevant work on non-linear localization). It was also found that this $\mathbf{S}_1 \times \mathbf{S}_{N-1}$ branch leads to the maximum $\|s\|_{ss}$ and it results in a mild saturation of $\|yy'\|_{ss}$ after bifurcation.

Designers of absorber systems can refer to the information provided herein in order to obtain refined estimates of system performance before testing. However, it is recognized that other effects may have equal or greater influence on the overall system behavior. Of particular importance is the level of absorber damping; while generally small in practice, it is difficult to measure and may vary during operation (due to wear, temperature

differences, etc.). It is interesting to note that when designing an absorber system, it is desirable to keep this damping as small as possible in order to keep the absorber oscillating in an out-of-phase fashion relative to the disturbing torque. This offers optimal torque counteraction if the absorbers move in unison. However, for a multiple absorber system, a lower damping level will cause the bifurcation to a non-unison response at a smaller level of the disturbing torque level, causing a potentially dramatic decrease in the applicable torque range.

As stated in the introduction, this investigation is only the first step in the study of unison absorber motions. To be of any practical use, the results must be extended to include: other absorber paths, including the widely-used, intentionally mis-tuned circular path; the effects of multiple harmonics in the torque; rotor flexibility and the distribution of torque along the axis of rotation; and mistuning, i.e., symmetry breaking, to name a few. Preliminary simulations that include small mistunings among the absorbers indicate that the individual absorber dynamics can be drastically altered by mistunings of the order of 1%. However, it is also observed that the overall $\|s\|_{ss}$'s and $\|yy'\|_{ss}$'s are quite robust to such changes. An investigation of these effects will bring the research squarely into the active realm of mode localization (Happawana *et al*. [20]; Hodges [21]; Pierre and Dowell [22]; Vakakis and Cetinkaya [19]).

ACKNOWLEDGMENTS

The authors are grateful to Professor Anil Bajaj of Purdue, Professor Tim Healey of Cornell, and Dr. Tim Whalen of NIST for their assistance with symmetric bifurcation theory. This work was supported in part by a grant from the National Science Foundation.

REFERENCES

1. B. C. Carter 1929 *British Patent No*. 337446.
2. W. Ker Wilson 1968 *Practical Solution of Torsional Vibration Problems*. London: Chapman and Hall Ltd; third edition, **IV**, Chapter XXX.
3. J. P. Den Hartog 1938 In *Stephen Timoshenko* 60*th Anniversary*, New York: The Macmillan Company; **17–26**, Tuned pendulums as torsional vibration eliminators.
4. D. E. Newland 1964 *American Society of Mechanical Engineers*, *Journal of Engineering for Industry* **86**, 257–263. Nonlinear aspects of the performance of centrifugal pendulum vibration absorbers.
5. M. Sharif-Bakhtiar and S. W. Shaw 1992 *American Society of Mechanical Engineers*, *Journal of Vibration and Acoustics* **114**, 305–311. Effects of nonlinearities and damping on the dynamic response of a centrifugal pendulum absorber.
6. J. F. Madden 1980 *United States Patent No*. 4218187. Constant frequency bifilar vibration absorber.
7. H. H. Denman 1992 *Journal of Sound and Vibration* **159**, 251–277. Tautochronic bifilar pendulum torsion absorbers for reciprocating engines.
8. V. J. Borowski, H. H. Denman, D. L. Cronin, S. Shaw, J. P. Hanisko, L. T. Brooks, D. A. Milulec, W. B. Crum and M. P. Anderson 1991 *The Engineering Society for Advanced Mobility Land*, *Sea*, *Air and Space*, *SAE Technical Paper Series* 911876. Reducing vibration of reciprocating engines with crankshaft pendulum vibration absorbers.
9. S. W. Shaw and C.-T. Lee 1995 *Smart Structures*, *Nonlinear Vibration*, *and Control* (editors A. Guran and D. J. Inman), New Jersey: Prentice Hall; pp. 247–309. On the nonlinear dynamics of centrifugal pendulum vibration absorbers.
10. C.-T. Lee, S. W. Shaw and V. T. Coppola 1996 to appear, *American Society of Mechanical Engineers*, *Journal of Vibration and Acoustics*. A subharmonic vibration absorber for rotating machinery.
11. C.-P. Chao, S. W. Shaw and C.-T. Lee 1997 *American Society of Mechanical Engineers*,

Journal of Applied Mechanics **64,** 149–156. Stability of the unison response for a rotating system with multiple centrifugal pendulum vibration absorbers.
12. M. Golubitsky, I. Stewart and D. G. Schaeffer 1988 *Singularities and Groups in Bifurcation Theory*. New York: Springer-Verlag; II.
13. D. S. Dummit and R. M. Foote 1991 *Abstract Algebra*. Englewood Cliffs, NJ: Prentice Hall.
14. D. L. Cronin 1992 *Mechanism and Machine Theory* **27**, 517–533. Shake reduction in an automobile engine by means of crankshaft-mounted pendulums.
15. T. J. Healey and J. A. Treacy 1991 *International Journal for Numerical Methods in Engineering* **31**, 265–285. Exact block diagonalization of large eigenvalue problems for structures with symmetry. Pitman, Boston.
16. G. Cicogna 1981 *Lettere al Nuovo Cimento* **31**, 600–602. Symmetry breakdown from bifurcations.
17. A. Vanderbauwhede 1982 *Research Notes in Mathematics* **75**. Local bifurcation and symmetry.
18. J. Stoer and R. Bulirsch 1976 *Introduction to Numerical Analysis*. New York: Springer-Verlag; second edition.
19. A. F. Vakakis and T. K. Centikaya 1993 *SIAM Journal of Applied Mathematics* **53**, 265–282. Mode localization in a class of multi-degree-of-freedom systems with cyclic symmetry.
20. G. S. Happawana, A. K. Bajaj and O. D. I. Nwokah 1993 *Journal of Sound and Vibration* **160**, 225–242. A singular perturbation analysis of eigenvalue veering and modal sensitivity in perturbed linear periodic systems.
21. C. H. Hodges 1982 *Journal of Sound and Vibration* **82**, 411–424. Confinement of vibration by structural irregularity.
22. C. Pierre and E. H. Dowell 1987 *Journal of Sound and Vibration* **114**, 549–564. Localization of vibrations by structure irregularity.

APPENDIX A: THE NON-TRUNCATED AVERAGED EQUATIONS

The non-truncated (in terms of amplitudes) averaged equations are given by

$$\mathrm{d}r_i/\mathrm{d}\theta = \varepsilon\Big\{-\tfrac{1}{2}\tilde{\mu}_a r_i + (\tilde{\Gamma}_\theta/n)\cos\varphi_i F_1(r_i) + \frac{1}{N}\sum_{j\neq i}[\tfrac{1}{4}n^3 r_i r_j^2 \sin(2\alpha_{ji}) - nr_j G_1(r_i, r_j, \alpha_{ji}) - n(n^2+n^4)r_j^3 H_1(r_i, r_j, \alpha_{ji})]\Big\} + \mathcal{O}(\varepsilon^2), \quad \text{(A1a)}$$

$$\mathrm{d}\varphi_i/\mathrm{d}\theta = \varepsilon\Big\{(-\tilde{\Gamma}_\theta/nr_i)\sin\varphi_i F_2(r_i) + \frac{1}{N}(\tfrac{1}{4}n^5 r_i^2 - \tfrac{1}{2}n) + \frac{1}{N}\sum_{j\neq i}\left[-\tfrac{1}{4}n^3 r_j^2\cos(2\alpha_{ji}) - \frac{nr_j}{ri}G_2(r_i, r_j, \alpha_{ji}) - n(n^2+n^4)\frac{r_j^3}{r_i}H_2(r_i, r_j, \alpha_{ji})\right]\Big\} + \mathcal{O}(\varepsilon^2), \qquad 1 \leqslant i \leqslant N. \quad \text{(A1b)}$$

where

$$\alpha_{ji} = \varphi_j - \varphi_i$$

$$F_1(r_i) = \frac{1}{2\pi}\int_0^{2\pi} \sin^2 x[1 - (n^2+n^4)r_i^2\cos^2 x]^{1/2}\,\mathrm{d}x,$$

$$F_2(r_i) = \frac{1}{2\pi}\int_0^{2\pi} \cos^2 x[1 - (n^2+n^4)r_i^2\cos^2 x]^{1/2}\,\mathrm{d}x,$$

$$G_1(r_i, r_j, \alpha_{ji}) = \frac{1}{2\pi}\int_0^{2\pi} \cos(x)\sin(x-\alpha_{ji})[1 - (n^2+n^4)r_j^2\cos^2 x]^{1/2}$$

$$\times [1 - (n^2 + n^4)r_i^2 \cos^2(x - \alpha_{ji})]^{1/2}\, \mathrm{d}x,$$

$$G_2(r_i, r_j, \alpha_{ji}) = \frac{1}{2\pi}\int_0^{2\pi} \cos(x)\cos(x - \alpha_{ji})[1 - (n^2 + n^4)r_j^2 \cos^2 x]^{1/2}$$

$$\times [1 - (n^2 + n^4)r_i^2 \cos^2(x - \alpha_{ji})]^{1/2}\, \mathrm{d}x,$$

$$H_1(r_i, r_j, \alpha_{ji}) = \frac{1}{2\pi}\int_0^{2\pi} \cos(x)\sin^2(x)\sin(x - \alpha_{ji})\left[\frac{1 - (n^2 + n^4)r_i^2 \cos^2(x - \alpha_{ji})}{1 - (n^2 + n^4)r_j^2 \cos^2 x}\right]^{1/2} \mathrm{d}x,$$

$$H_2(r_i, r_j, \alpha_{ji}) = \frac{1}{2\pi}\int_0^{2\pi} \cos(x)\sin^2(x)\cos(x - \alpha_{ji})\left[\frac{1 - (n^2 + n^4)r_i^2 \cos^2(x - \alpha_{ji})}{1 - (n^2 + n^4)r_j^2 \cos^2 x}\right]^{1/2} \mathrm{d}x.$$

APPENDIX B: JUSTIFICATION OF $\tilde{\bar{\psi}} \simeq \tilde{\bar{\psi}}_j$, $\forall 2 \leqslant i, j \leqslant N$

In order to justify the assumption $\tilde{\bar{\psi}} \simeq \tilde{\bar{\psi}}_j$, $\forall 2 \leqslant i, j \leqslant N$, in the post-bifurcation stage, the transformation with η_1 capturing the dynamics in **V** and the remaining $\eta_i (2 \leqslant i \leqslant N)$ capturing the dynamics in **W**, where all η_i's are **orthogonal** to each other, is employed in place of transformation (16). Then, by also introducing the angular transformation

$$\eta_i = \varrho_i \cos(\tau_i - n\theta) \qquad \text{and} \qquad \eta_i' = n\varrho_i \sin(\tau_i - n\theta), \qquad 2 \leqslant i \leqslant N, \tag{B1}$$

and proceeding along the usual lines for the application of averaging, one arrives at the following steady state conditions, in place of equations (23),

$$0 = \frac{-\tilde{\mu}_a \tilde{\varrho}_i}{2} + (\tilde{\Gamma}_\theta^2 \tilde{\varrho}_i / 4n)\sin(2\tilde{\tau}_i), \quad 0 = \tilde{\Gamma}_\theta^2 \tilde{\varrho}_i 4n \cos(2\tilde{\tau}_i) - \frac{(N-1)n^3}{4}\tilde{\varrho}_i\left(\sum_{j=2}^{N} \tilde{\varrho}_j^2\right). \tag{B2a, B2b}$$

where $\tilde{\varrho}$ and $\tilde{\tau}$ are the approximate (averaged and truncated) versions of ϱ and τ. The above equations give

$$\tilde{\tau}_i = \tilde{\tau}_j, \qquad (\mathrm{mod}\ \pi)\forall i, j \in \mathcal{N}. \tag{B3}$$

By the definitions of the ξ_i's and the η_i's, each ξ_i with $i \in \mathcal{N}$ is a linear combination of the η_i's with $i \in \mathcal{N}$. Hence, $\tilde{\bar{\psi}}_i = \tilde{\bar{\psi}}_j$, $(\mathrm{mod}\ \pi)\forall i, j \in \mathcal{N}$. Now, choose an arbitrary $i_0 \in \mathcal{N}$. For all $j_0 \in \mathcal{N}$ with $\tilde{\bar{\psi}}_{i_0} = \tilde{\bar{\psi}}_{j_0} + \pi$, $(\mathrm{mod}\ 2\pi)$, replace $(\tilde{\rho}_{j_0}, \tilde{\bar{\psi}}_{j_0})$ by $(-\tilde{\rho}_{i_0}, \tilde{\bar{\psi}}_{i_0})$ to equivalently represent the signal s_{j_0}, and then proceed with the analysis in section 4. One finds that the results are the same as those obtained if $\tilde{\bar{\psi}}_i = \tilde{\bar{\psi}}_j \forall i, j \in \mathcal{N}$ is assumed.

APPENDIX C: PROOF OF Trace [A + (N − 2)B] < 0 AND Det [A + (N − 2)B] > 0 AS $\hat{\tilde{\rho}} \to 0^+$

In section 4.3., it was claimed that the $\mathbf{S}_1 \times \mathbf{S}_{N-1}$ branch, with $\tilde{\bar{\psi}} \simeq -3\pi/4$, leads to Trace [A + (N − 2)B] < 0 and Det [A + (N − 2)B] > 0 as $\tilde{\rho} \to 0^+$ near the bifurcation point. Through a non-trivial computation it can be shown that

$$\mathrm{Trace}\,[\mathrm{A} + (N-2)\mathrm{B}] = -\tilde{\mu}_a < 0,$$

$$\mathrm{Det}\,[\mathrm{A} + (N-2)\mathrm{B}] = \tfrac{1}{256}\{4n^6(N-1)^2N^2\tilde{\rho}^4 + 7\tilde{\mu}_a^2(N-2)^2(n^2+n^4)^2\tilde{\rho}^2\tilde{\rho}_1^2$$
$$+ 16(N-2)\tilde{\mu}_a^2(n^2+n^4)\hat{\rho}\hat{\rho}_1\cos(\hat{\bar{\psi}} - \hat{\bar{\psi}}_1)$$

$$- 8(N-2)^2\tilde{\mu}_a^2(n^2+n^4)^2\hat{\rho}^2\hat{\rho}_1^2\cos(2\hat{\psi}-2\hat{\psi}_1)$$

$$-16(N-2)(N-1)N\tilde{\mu}_a n^3(n^2+n^4)\hat{\rho}^3\hat{\rho}_1\sin(\hat{\psi}-\hat{\psi}_1)\}. \quad \text{(C1)}$$

On the $\mathbf{S}_1 \times \mathbf{S}_{N-1}$ solution branch with $\hat{\psi} \simeq -3\pi/4$,

$$\cos(\hat{\psi}-\hat{\psi}_1) \simeq 1/\sqrt{2}, \qquad \cos(2\hat{\psi}-2\hat{\psi}_1) \simeq 0, \qquad \text{and} \qquad \sin(\hat{\psi}-\hat{\psi}_1) \simeq -1/\sqrt{2}. \quad \text{(C2)}$$

Thus, Det $[A + (N-2)B] > 0$ on this branch as $\hat{\rho} \to 0^+$ near the bifurcation point.

APPENDIX D: THE LOW ORDER APPROXIMATION OF $yy'(\theta)$

To obtain the expressions for $yy'(\theta)$ in equation (37), a simplification is carried out in two steps. First, it can be shown that

$$n^2\xi_1 + \tilde{\Gamma}_\theta \sin(n\theta) \simeq 0 \quad \text{(D1)}$$

by incorporating the approximate steady state solutions for ρ_1 and ψ_1 in equations (22). Second, the remaining term is reduced based on the corresponding truncated steady state equations (23). It can be shown that before the bifurcation the absorber motions undergo unison motion, which yields

$$\frac{2n^2}{N}\sum_{j=1}^{N} s_j s_j' = 2n^2\xi_1\xi_1' = n^3\tilde{\rho}_1^2\sin(2\tilde{\psi}_1 - 2n\theta). \quad \text{(D2)}$$

After the bifurcation, the transformations in equations (17) and (19) yield

$$\frac{2n^2}{N}\sum_{j=1}^{N} s_j s_j' = n^3\Bigg[\tilde{\rho}_1^2\sin(2\tilde{\psi}_1 - 2n\theta) - (N-1)\sum_{j\neq 1}\tilde{\rho}_j^2\sin(2\tilde{\psi}_j - 2n\theta)$$

$$+ \sum_{j,k\neq 1 \text{ and } j\neq k} 2\tilde{\rho}_j\tilde{\rho}_k\sin(\tilde{\psi}_j + \tilde{\psi}_k - 2n\theta)\Bigg]. \quad \text{(D3)}$$

Utilizing some trigonometric identities and the approximate solutions in equations (22):

$$\text{R.S of (D3)} = \cos(2\tilde{\psi}_i - 2n\theta)\Bigg\{n^3\tilde{\rho}_1^2\sin(2\tilde{\psi}_i)$$

$$+ n^3\sum_{j\neq 1,i}\{2\hat{\rho}_i\hat{\rho}_j\sin(\hat{\psi}_i - \hat{\psi}_j) - (N-1)\hat{\rho}_j^2\sin[2(\hat{\psi}_i - \hat{\psi}_j)]\}$$

$$+ n^3\sum_{j,k\neq 1,i \text{ and } j\neq k} 2\tilde{\rho}_j\tilde{\rho}_k\sin(2\tilde{\psi}_i - \tilde{\psi}_j - \tilde{\psi}_k)\Bigg\}$$

$$+ \sin(2\tilde{\psi}_i - 2n\theta)\Bigg\{n^3\tilde{\rho}_1^2\cos(2\tilde{\psi}_i) + (N-1)n^3\tilde{\rho}_i^3$$

$$+ n^3 \sum_{j \neq 1,i} \{2\tilde{\rho}_i\tilde{\rho}_j \cos(\tilde{\psi}_i - \tilde{\psi}_j) - (N-1)\tilde{\rho}_j^2 \cos[2(\tilde{\psi}_i - \tilde{\psi}_j)]\}$$

$$+ n^3 \sum_{j,k \neq 1,i \text{ and } j \neq k} 2\tilde{\rho}_j\tilde{\rho}_k \cos(2\tilde{\psi}_i - \tilde{\psi}_j - \tilde{\psi}_k)\Big\}, \qquad 2 \leqslant i \leqslant N. \tag{D4}$$

Incorporating the truncated averaged equations in equation (23) yields

$$\text{R.S of (D4)} = 2\tilde{\mu}_a \cos(2\tilde{\psi}_i - 2n\theta), \qquad 2 \leqslant i \leqslant N. \tag{D5}$$

Based on the results in Appendix B, one finds

$$2\hat{\mu}_a \cos(2\tilde{\psi}_i - 2n\theta) = 2\tilde{\mu}_a \cos(2\tilde{\psi} - 2n\theta), \qquad 2 \leqslant i \leqslant N,$$

after the bifurcation.